13 Direct Diffusion Studies

13.1 Direct *versus* Indirect Methods

There are numerous experimental methods for studying diffusion in solids. They can be grouped roughly into two major categories (see Table 13.1).

Direct methods are based on the laws of Fick and the phenomenological definition of the diffusion coefficient therein. They are sensitive to long-range diffusion and in this sense they are macroscopic.

The radiotracer method is the standard technique for the study of self- and solute diffusion, if radioisotopes with suitable half-lives are available. The tracer method is element-selective and due to the use of nuclear counting facilities highly sensitive. It can cover a large range of diffusivities provided that both mechanical and sputter sectioning techniques are used for depth profiling. Further profiling techniques for diffusion studies are secondary ion mass

Table 13.1. Survey of experimental methods for direct and indirect diffusion studies in solids

Direct methods	Indirect methods
Tracer diffusion plus depth profiling	**Mechanical spectroscopy** (after effect, internal friction, Gorski effect)
Chemical diffusion plus profiling	**Magnetic relaxation** (for ferromagnetc materials)
Profiling techniques:	**Nuclear magnetic relaxation** (NMR):
- Mechanical and sputter profiling	- Line-shape spectroscopy
- Secondary ion mass spectrometry (SIMS)	- Spin lattice relaxation spectroscopy
- Electron microprobe analysis (EMPA)	- Spin alignment experiments (SAE)
- Auger electron spectroscopy (AES)	**Impedance spectroscopy** (IS) for ion conductors
Spreading resistance profiling (SRP) for semiconductors	**Mössbauer spectroscopy** (MBS)
Rutherford backscattering (RBS)	**Quasielastic neutron scattering** (QENS)
Nuclear reaction analysis (NRA)	
Field gradient NMR (FG-NMR)	
Pulsed fieldgradient NMR (PFG-NMR)	

spectrometry (SIMS), electron microprobe analysis (EMPA), Auger electron spectroscopy (AES). SIMS and AES both utilise sputter profiling and are appropriate for small diffusion distances and low diffusivities. AES is applicable for diffusion of foreign atoms, since it discriminates between different elements but not between isotopes of the same element. EMPA is the major tool for the study of chemical diffusion (interdiffusion) and suitable for relatively large diffusion coefficients, since the size of the specimen volume excited by the electron beam limits the depth resolution. Rutherford back scattering (RBS) or nuclear reaction analysis (NRA) are both nuclear techniques, which use ion beams of several MeV energy for profile analysis. RBS is particular suitable for heavy solutes in a light solvent whereas NRA is appropriate for some light solutes including hydrogen. A prerequisite for NRA studies is a nuclear reaction with a narrow resonance. The penetration depth and energy straggling of the ion beam limit RBS and NRA to small diffusivities. Spreading resistance profiling (SRP) of dopant diffusion profiles in semiconductors is direct in the sense that it provides a depth profile of the spreading resistance. However, some transformation is needed to convert spreading resistance to dopant concentration. Usually, NMR techniques are indirect (see below). However, field-gradient NMR, either with static field gradients (FG-NMR) or with pulsed field gradients (PFG-NMR), are methods that permit diffusivity measurements without referring to a microscopic model.

Indirect methods are not directly based on the laws of Fick. Indirect methods usually study phenomena which are influenced by the diffusion jumps of atoms.

Some of these methods are sensitive to one or a few atomic jumps only. Quantities such as relaxation times, relaxation rates, or line-widths are measured and the mean residence time of the diffusing atoms, $\bar{\tau}$, is deduced therefrom. A microscopic model of the atomic jump process is needed to deduce the diffusivity via the Einstein-Smoluchowski relation (see Chap. 4). In simple cases, the (uncorrelated) diffusivity D_E is given by

$$D_E = \frac{d^2}{6\bar{\tau}}\,, \tag{13.1}$$

where d denotes the length of an atomic jump.

The numbers of atomic jumps performed by the diffusing species during anelastic or magnetic after-effect measurements (e.g., Snoek or Zener effect) are typically of the order of one. Internal friction studies are particularly sensitive to diffusion processes, when the atomic jump rate, $1/\bar{\tau}$, is comparable with the vibration frequency of the internal friction device. When applicable, these techniques can monitor very small to small diffusion coefficients. The Gorski effect is an anelastic after-effect, which can be observed in hydrogen-metal systems. Its origin is the hydrogen redistribution in a strained sample. The associated after-effect can be monitored because hydrogen diffusion is a very fast process.

Among the nuclear methods, nuclear magnetic relaxation (NMR) covers the widest range of diffusivities. Spin-alignment experiments (SAE), line-shape spectroscopy, and spin-lattice relaxation spectroscopy can be used. Favourable are materials with large gyromagnetic ratios and small non-diffusive contributions to line-width or relaxation rates. Mössbauer spectroscopy (MBS) requires a suitable Mössbauer isotope. The usual workhorse of MBS is ^{57}Fe, which permits studies of Fe diffusion. There is a short list of further Mössbauer probes such as ^{119}Sn, ^{151}Eu, and ^{161}Dy. Quasielastic neutron scattering (QENS) is applicable to isotopes with large enough quasi-elastic scattering cross sections. Both techniques are limited to relatively fast diffusion processes. The main virtues of MBS and QENS are that these techniques can unravel microscopic information such as jump length and jump direction of the diffusing atoms.

Impedance spectroscopy (IS) measures the complex conductivity of ion-conducting materials as a function of the frequency. For materials in which only one type of ion contributes to the dc conductivity, Eq. (11.26) can be used to 'translate' the dc conductivity, σ_{dc}, into a charge diffusion coefficient of the ions, D_σ (see Chap. 11).

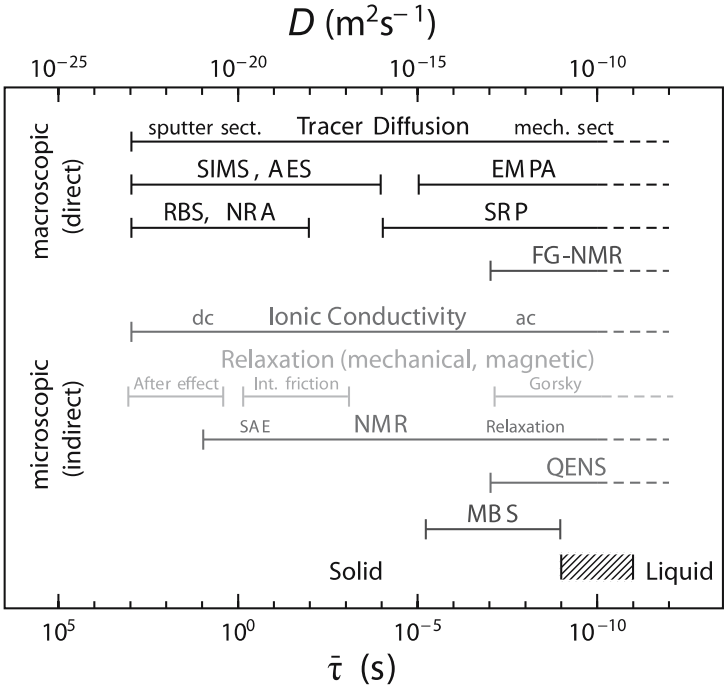

Fig. 13.1. Typical ranges of the diffusivity D and the mean residence time $\bar{\tau}$ of direct and indirect methods for diffusion studies

Figure 13.1 shows typical ranges of diffusivity (D: *upper abscissa*) and mean residence time ($\bar{\tau}$: *lower abscissa*) for direct and indirect methods, respectively. D and $\bar{\tau}$ have been converted via Eq. (13.1), adopting a typical jump length d in solids of some tenths of a nanometer. The length scale for the diffusion processes which are probed by IS and NMR varies with the applied measuring frequency. Thus a combination of various techniques and/or experimental devices may be desirable.

The present chapter is devoted to direct methods. Diffusion of atoms in a certain direction x is described by one of the following versions of Fick's second law (see Chaps. 2 and 10)

$$\frac{\partial C}{\partial t} = D\frac{\partial^2 C}{\partial x^2} \quad \text{or} \quad \frac{\partial C}{\partial t} = \frac{\partial}{\partial x}\left[\tilde{D}(C)\frac{\partial C}{\partial x}\right]. \tag{13.2}$$

The first version corresponds to a concentration-independent diffusivity. As outlined below, in experiments with trace elements very tiny amounts of the diffusing species can be studied and the chemical composition of the sample is unchanged. The second version is applicable for a concentration-dependent diffusion coefficient, $\tilde{D}(c)$, denoted as the *interdiffusion- or chemical diffusion coefficient* (see Chap. 10). We discuss relaxation and internal friction methods based on the anelastic behaviour of materials in Chap. 14, the nuclear methods NMR, MBS, and QENS in Chap. 15, and the electrical methods IS and SRP in Chap. 16. For further details the reader may consult textbooks [1–3], reviews [4, 5], and conference proceedings [6–9].

13.2 The Various Diffusion Coefficients

Before discussing experimental methods in detail, we describe situations which entail various types of diffusion coefficients. In this section, we distinguish the various diffusion coefficients by lower and upper indices. We drop the indices in the following text again, whenever it is clear which diffusion coefficient is meant. We concentrate on lattice (bulk) diffusion in unary and binary systems. Diffusion in ternary systems produces complexities, which are not treated in this book. We focus on lattice diffusion since diffusion along grain boundaries and dislocations is considered separately in Chaps. 32 and 33.

13.2.1 Tracer Diffusion Coefficients

In diffusion studies with trace elements (labelled by their radioactivity or by their isotopic mass) tiny amounts of the diffusing species (in the ppm range or even less) can be used. Although in a diffusion experiment a concentration gradient of the trace element is necessary, the total tracer concentration can be kept so small that the overall composition of the sample during the

investigation practically does not change. From an atomistic viewpoint this implies that a tracer atom is not influenced by other tracer atoms. The analysis of such a diffusion experiment yields a *tracer diffusion coefficient*, which is independent of tracer concentration. Tracers are appropriate to study self-diffusion of matrix atoms. They can also be used to study diffusion of foreign atoms under very dilute conditions. The latter phenomenon is called *impurity diffusion*. The expressions *foreign diffusion* or *solute diffusion* are also used.

Self-diffusion: The diffusion of A atoms in a solid element A is called *self-diffusion*. Studies of self-diffusion with tracers utilise an isotope A^* of the same element. A typical initial configuration for a tracer self-diffusion experiment is illustrated in Fig. 13.2a. The *tracer self-diffusion coefficient* $D_A^{A^*}$ is obtained from the diffusion broadening of a narrow initial distribution.

The connection between the macroscopically defined tracer self-diffusion coefficient and the atomistic picture of diffusion is the *Einstein-Smoluchowski relation* discussed in Chap. 4. In simple cases, it reads

$$D_A^{A^*} = f D_E \quad \text{with} \quad D_E = \frac{d^2}{6\bar{\tau}}\,, \tag{13.3}$$

where d denotes the jump length and $\bar{\tau}$ the mean residence time of an atom on a particular but arbitrary site of the crystal. Equation (13.3) is applicable for cubic structures when only jumps to nearest-neighbour sites occur. f is the tracer correlation factor discussed in Chap. 7. For self-diffusion in cubic crystals f is usually a known numeric factor, which depends on the lattice geometry and the diffusion mechanism. In some textbooks the quantity D_E is denoted as the *Einstein diffusion coefficient*. In the author's opinion, the notation Einstein diffusion coefficient is misleading, since the original Einstein-Smoluchowski equation relates the total macroscopic mean square displacement of atoms to the diffusion coefficient (see Chap. 4), in which correlation effects are included.

In a homogeneous binary $A_X B_{1-X}$ alloy or compound two tracer self-diffusion coefficients for A^* and B^* tracer atoms can be measured using the initial configuration displayed in Fig. 13.2b. We denote the corresponding tracer diffusion coefficients by $D_{A_X B_{1-X}}^{A^*}$ and $D_{A_X B_{1-X}}^{B^*}$. In general, the two tracer diffusivities are not equal:

$$D_{A_X B_{1-X}}^{A^*} \neq D_{A_X B_{1-X}}^{B^*}.$$

Depending on the specific alloy system one component will be more mobile than the other. The difference depends on the crystal structure of the material, on the atomic mechanisms which mediate diffusion, and on the constituents themselves. For example, in B2 structured intermetallic compounds the tracer diffusivities of the constituents are usually similar, whereas in $L1_2$ or DO_3 structured compounds the component diffusivities can be very different (see [10–12] and Chap. 20). In ionic crystals and ceramics the diffusivities of the components also can differ significantly (see Chaps. 26 and 27). Of

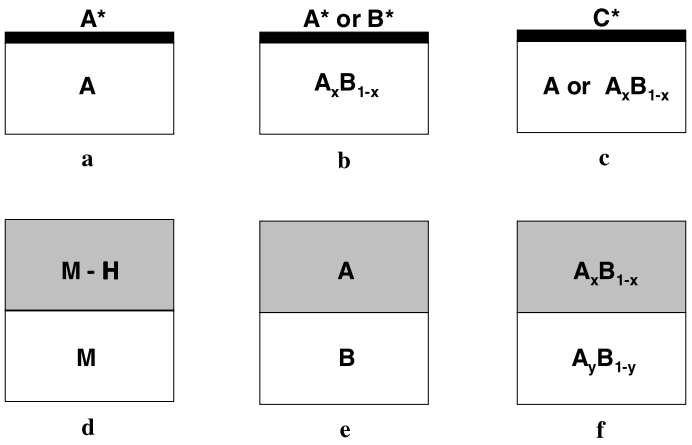

Fig. 13.2a–f Initial configurations for direct diffusion studies: **a**) Thin layer of A^* on solid A: tracer self-diffusion in pure elements. **b**) Thin layer of A^* or B^* on homogeneous A-B alloy: tracer self-diffusion of alloy components. **c**) Thin layer of C^* on solid A or on a homogeneous alloy: Impurity diffusion. **d**) Diffusion couple between metal-hydrogen alloy and a pure metal. **e**) Diffusion couple between pure end-members. **f**) Diffusion couple between two homogeneous alloys

course, both component diffusivities are also functions of the thermodynamic variables temperature and pressure and in general also depend on the composition.

Impurity Diffusion: When the diffusion of a trace solute C^* in a monoatomic solvent A or in a homogeneous binary solvent A_XB_{1-X} (Fig. 13.2c) is measured, the tracer diffusion coefficients

$$D_A^{C^*} \text{ and } D_{A_XB_{1-X}}^{C^*}$$

are obtained. These diffusion coefficients are denoted as the *impurity diffusion coefficients* or sometimes also as the *foreign diffusion coefficients*.

13.2.2 Interdiffusion and Intrinsic Diffusion Coefficients

For interdiffusion studies on binary alloys, diffusion couples are formed consisting either of two elements from a continuous solid solution alloy or of two homo-phase alloys with different compositions (A_XB_{1-X} and A_YB_{1-Y}) within the same phase field (Fig. 13.2 e and f). Usually the thicknesses of the couple members are chosen large as compared to the average diffusion length. Then, each couple member can be considered to be semi-infinite. Some typical examples are:

– Pure end-member diffusion couples consisting of two slices of pure elements joined together (Ni|Pd, Au|Ag, Si|Ge, ...).

- Incremental diffusion couples consisting of two slices of homogenous alloys joined together
  ($Fe_{75}Al_{25}|Fe_{60}Al_{40}$, $Ni_{50}Pd_{50}|Ni_{70}Pd_{30}$, $Ni|Ni_{70}Pd_{30}$, ...).
- Diffusion couples which involve solutions of hydrogen
  (Pd-H|Pd, $Ag_{1-X}H_X|Ag_{1-Y}H_Y$, ...).

During hydrogen interdiffusion the metal atoms are practically immobile. Then the intrinsic diffusion coefficient and the chemical diffusion coefficient of hydrogen are identical.

Interdiffusion: The phenomenon of *interdiffusion* or *chemical diffusion* has been discussed in Chap. 10. We have seen that the interdiffusion coefficient $\tilde{D}$ can be deduced either by a Boltzmann-Matano analysis for systems without volume change or for systems with volume changes from a Sauer-Freise type analysis of the experimental concentration-distance profile. Using one of these methods, an interdiffusion coefficient

$$\tilde{D} = \tilde{D}(C)$$

for each composition C in the diffusion zone is obtained (see Chap. 10). $\tilde{D}$ characterises the intermixing of A and B atoms.

Intrinsic Diffusion: The intrinsic diffusion coefficients D_A^I and D_B^I describe diffusion of the components A and B of a binary alloy relative to the lattice planes. As discussed in Chap. 10, a determination the intrinsic diffusivities requires two measurements. The *Kirkendall velocity*, v_K, and the interdiffusion coefficient, $\tilde{D}$, permit to deduce intrinsic diffusivities as described in Chap. 10. Either the Darken equations or the more precise Darken-Manning equations can be used.

13.3 Tracer Diffusion Experiments

Many of the reliable diffusion studies on solids have been performed by radiotracer techniques as evidenced in textbooks [1–3], reviews [4, 5, 10–12] and conference proceedings [6–9]. Due to the high sensitivity of nuclear counting facilities, radiotracer studies are often superior to other techniques. A very important advantage is the fact that self-diffusion – the most basic diffusion process in a solid material – can be studied in a straightforward manner using radioisotopes of matrix atoms. Then, the tracer self-diffusion coefficient is obtained. Foreign atom diffusion studies can also be performed with tiny amounts of tracer. Typical tracer concentrations are less or even much less than a ppm, if radioisotopes with high specific activity are used. In this way, diffusion in a chemically homogeneous solid can be investigated. Complications due to chemical gradients play no rôle and the thermodynamic factor equals unity. In a tracer diffusion experiment atoms are usually labelled by their radioactivity. When stable isotopes are used as tracers the 'label' is

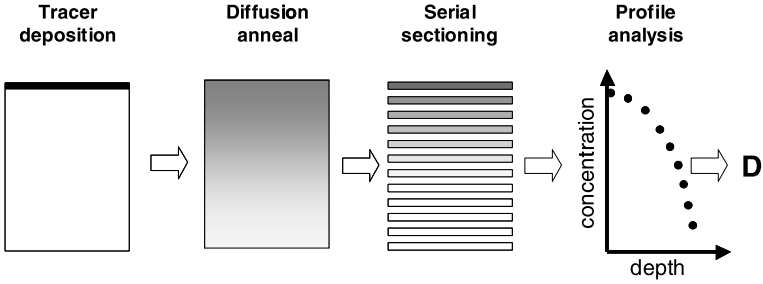

Fig. 13.3. Schematic illustration of the tracer method: The major steps – deposition of the tracer, diffusion anneal, serial sectioning, and evaluation of the penetration profile – are indicated

the isotopic mass. Sometimes, in the case of impurity diffusion atoms are labelled just by their chemical nature. The major steps of a tracer diffusion experiment are indicated in Fig. 13.3.

Preparation of a diffusion sample usually involves preparation of a flat, strain-free surface. Polishing of metals, intermetallics, semiconductors, and glasses is usually performed by standard metallographic procedures. Soft materials such as organic crystals or polymers can be cut with a microtome. Mechanical methods produce the best flatness but introduce strain. Etching or electropolishing and/or a pre-diffusion anneal should be used to remove cold-worked material.

The tracer is deposited onto the polished, flat surface of the diffusion sample. Evaporation, dripping of a liquid solution, and electrodeposition of the radiotracer onto the surface are the major deposition techniques. Complete homogeneity of the deposit is not necessary as long as iregularties in its thickness are small as compared to the mean diffusion length and as long as the same sample area is counted in each section [13]. Implantation of the radioisotope is more laborious but offers sometimes advantages [4, 14]: for example, tracer hold-up by surface oxide layers can be avoided by implantation.

Following the tracer deposition, an isothermal diffusion anneal is performed at temperature T for some diffusion time t. During the diffusion anneal the sample is usually encapsulated in a quartz ampoule under vacuum or inert atmosphere (e.g., Ar). For temperatures below 1500 K quartz ampoules and resistance furnaces are frequently used. For higher temperatures more sophisticated annealing techniques (e.g., electron-beam heating) are necessary.

Suppose that a thin layer of tracer atoms (M atoms per unit area) has been deposited at the surface $x = 0$ of a semi-infinite sample. Let us further suppose that tracer losses and tracer hold-up at the surface can be avoided. Then, the concentration distribution after a diffusion anneal is described by (see Chap. 3)

$$C(x,t) = \frac{M}{\sqrt{\pi Dt}} \exp\left(-\frac{x^2}{4Dt}\right). \tag{13.4}$$

We recall that Eq. (13.4) is the *thin-film solution (Gaussian solution)* of Fick's second law and that the quantity $\sqrt{Dt}$ is a typical *diffusion length*.

An alternative possibility of tracer deposition is *ion-implantation* using an accelerator. Implantation can be a very suitable deposition technique for materials like Al, which readily form a thin oxide layer when exposed to air. After implantation the tracer atoms form a buried layer. For a fixed implantation energy their distribution as a function of range x is given by[1]

$$C(x,0) = \frac{M}{\sqrt{2\pi\Delta R_p}} \exp\left[-\frac{(x-R_p)^2}{4Dt}\right]. \tag{13.5}$$

R_p denotes the *mean projected range of implantation* and ΔR_p the *standard deviation of the projected range*. Both quantities depend on the implantation energy, on the tracer, and on the matrix. Typical values of R_p lie in the range 20 to 100 nm for implantation energies of 50 keV. A layer buried in great depth broadens during diffusion annealing to

$$C(x,t) = \frac{M}{\sqrt{2\pi\Delta R_p + 4Dt}} \exp\left[-\frac{(x-R_p)^2}{2\Delta R_p + 4Dt}\right]. \tag{13.6}$$

However, after implantation the tracer layer will usually be close to the sample surface. Then, Eq. (13.6) must be modified. If the surface acts either as a 'perfect mirror' or as a 'perfect sink' for tracer atoms the solution of Fick's second equation can be written as

$$C(x,t) = \frac{M}{\sqrt{2\pi\Delta R_p + 4Dt}} \left(\exp\left[-\frac{(x-R_p)^2}{2\Delta R_p + 4Dt}\right] \pm \exp\left[-\frac{(x+R_p)^2}{2\Delta R_p + 4Dt}\right]\right). \tag{13.7}$$

The minus-sign stands for a perfect sink and the plus-sign for a perfect reflection at $x = 0$. Both boundary conditions are approximations and may not always hold in practical cases. If this is the case, numerical solutions of Fick's equation should be used.

13.3.1 Profile Analysis by Serial Sectioning

The major task of a diffusion experiment is to study the concentration-depth profile and to deduce the diffusion coefficient by comparison with the corresponding solution of Fick's second law. Let us assume that the experimental conditions were chosen in such a way that the deposited layer is thin compared with the diffusion length $\sqrt{Dt}$. Then, the distribution after the diffusion anneal is described by Eq. (13.4).

[1] For simplicity reasons we neglect channelling effects. Channeling can be neglected if the direction of the implntation beam avoids directions of high crystal symmetry,

The best way to determine the resulting concentration-depth profile is serial sectioning of the sample and subsequent determination of the amount of tracer per section. To understand sectioning the reader should think in terms of isoconcentration contours. For lattice diffusion these are parallel to the original surface, on which the thin layer is deposited, and perpendicular to the diffusion direction. The most important criterion of sectioning is the parallelness of sections to the isococentration contours. For radioactive tracers the specific activity per section, $A(x)$, is proportional to the tracer concentration:

$$A(x) = kC(x)\,. \tag{13.8}$$

Here k is a constant, which depends on the nature and energy of the nuclear radiation and on the efficiency of the counting device. The specific activity is obtained from the section mass and the count rate. The latter can be measured in nuclear counting facilities such as γ- or β-counting devices. Usually, the count-rate must be corrected for the background count-rate of the counting device. For short-lived radioisotopes half-life corrections are also necessary. According to Eq. (13.4) a diagram of the logarithm of the specific activity *versus* the penetration distance squared is linear. From its slope, $(4Dt)^{-1}$, and the diffusion time the tracer diffusivity D is obtained.

In an ordinary thin-layer sectioning experiment, one wishes to measure diffusion over a drop of about three orders of magnitude in concentration. About twenty sections suffice to define a penetration profile. The section thickness Δx required to get a concentration decrease of three orders of magnitude over 20 sections is $\Delta x \approx \sqrt{Dt}/3.8$. Thicker sections should be avoided for the following reason: in a diffusion penetration profile the average concentrations (specific activities) per section are plotted *versus* the position of the distance of the center of each section from the surface. Errors caused by this procedure are only negligible if the sections are thin enough.

The radiotracer deposited on the front face of a sample may rapidly reach the side surfaces of a sample by surface diffusion or via transport in the vapour phase and then diffuse inward. To eliminate lateral diffusion effects, one usually removes about $6\sqrt{Dt}$ from the sample sides before sectioning. For studies of bulk diffusion, single crystalline samples rather than polycrystalline ones should be used to eliminate the effects of grain-boundary diffusion, which is discussed in Chap. 31. If no single crystals are available coarse-grained polycrystals should be used.

The following serial-sectioning techniques are frequently used for the determination of diffusion profiles:

Mechanical sectioning: For diffusion lengths, $\sqrt{Dt}$, of at least several micrometers mechanical techniques are applicable (for a review see [4]). Lathes and microtomes are appropriate for ductile samples such as some pure metals (Na, Al, Cu, Ag, Au, ...) or polymers. For brittle materials such as intermetallics, semiconductors, ionic crystals, ceramics, and inorganic glasses grinding is a suitable technique.

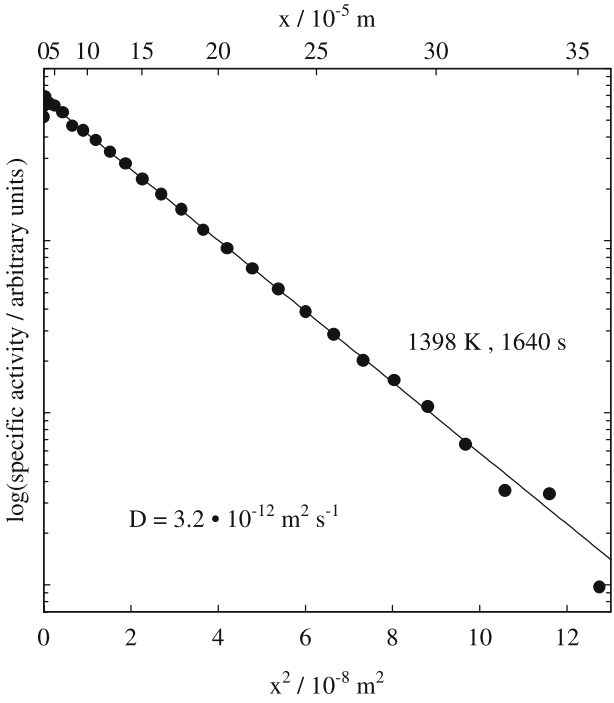

Fig. 13.4. Penetration profile of the radioisotope ^{59}Fe in Fe_3Si obtained by grinder sectioning [15]. The *solid line* represents a fit of the thin-film solution of Fick's second law

For extended diffusion anneals and large enough diffusivities, $D > 10^{-15}\,\mathrm{m^2\,s^{-1}}$, lathe sectioning can be used. Diffusivities $D > 10^{-17}\,\mathrm{m^2\,s^{-1}}$ are accessible via microtome sectioning. In cases where the half-life of the isotope permits diffusion anneals of several weeks, grinder sectioning can be used for diffusivities down to $10^{-18}\,\mathrm{m^2\,s^{-1}}$. Figure 13.4 shows a penetration profile of the radioisotope ^{59}Fe in the intermetallic Fe_3Si, obtained by grinder sectioning [15]. Gaussian behaviour as stated by Eq. (13.4) is observed over several orders of magnitude in concentration.

Ion-beam Sputter Sectioning (IBS): Diffusion studies at lower temperatures often require measurements of very small diffusivities. Measurements of diffusion profiles with diffusion lengths in the micrometer or sub-micrometer range are possible using sputtering techniques. Devices for serial sectioning of radioactive diffusion samples by ion-beam sputtering (IBS) are described in [16, 17]. Figure 13.6 shows a schematic drawing of such a device. Oblique incidence of the ion beam and low ion energies between 500 and 1000 eV are used to minimise knock-on and surface roughening effects. The sample (typically several mm in diameter) is rotated to achieve a homogeneous lateral sputtering rate. The sputter process is discussed in some detail below and

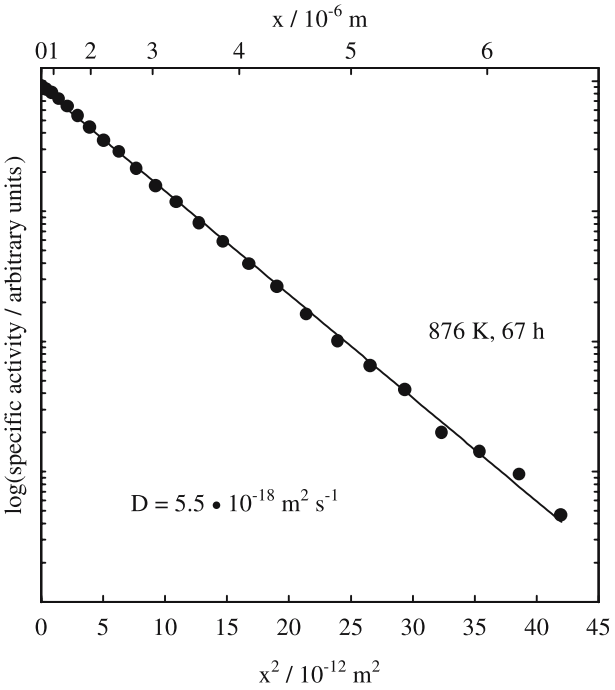

Fig. 13.5. Penetration profile of the radioisotope ^{59}Fe in Fe_3Al obtained by sputter sectioning [18]. The *solid line* represents a fit of the thin-film solution of Fick's second law

illustrated in Fig. 13.8, in connection with secondary ion mass spectroscopy (SIMS). An advantage of IBS devices lies in the fact that neutral atoms are collected, which comprise by far the largest amount (about 95 to 99 %) of the off-sputtered particles. In contrast, SIMS devices (see below) analyse the small percentage of secondary ions, which depends strongly on sputter- and surface conditions.

Sectioning of shallow diffusion zones, which correspond to average diffusion lengths between several ten nm and 10 μm, is possible using IBS devices. For a reasonable range of annealing times up to about 10^6 s, a diffusivity range between $10^{-23}\,m^2\,s^{-1}$ and $10^{-16}\,m^2\,s^{-1}$ can be examined. Depth calibration can be performed by measuring the weight loss during the sputtering process or by determining the depth of the sputter crater by interference microscopy or by profilometer techniques. The depth resolution of IBS and SIMS is limited by surface roughening and atomic mixing processes to about several nm. A penetration profile of ^{59}Fe in the intermetallic Fe_3Al [18], obtained with the sputtering device described in [17] is displayed in Fig. 13.5.

From diffusion profiles of the quality of Figs. 13.4 and 13.5, diffusion coefficients can be determined with an accuracy of a few percent. A determi-

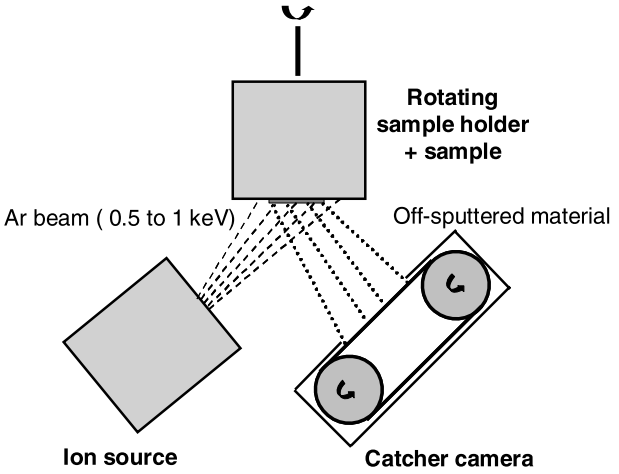

Fig. 13.6. Ion-beam sputtering device for serial sectioning of diffusion samples

nation of the absolute tracer concentration is not necessary since the diffusion coefficient is obtained from the slope, $-1/(4Dt)$, of such profiles.

Deviations from Gaussian behaviour in experimental penetration profiles (not observed in Figs. 13.4 and 13.5) may occur for several reasons:

1. *Grain-boundary diffusion*: Grain boundaries in a polycrystalline sample act as diffusion short-circuits with enhanced mobility of atoms. Grain boundaries usually cause a 'grain-boundary tail' in the deeper penetrating part of the profile (see Chap. 32 and [19]). In the 'tail' region the concentration of the diffuser is enhanced with respect to lattice diffusion. Then, one should analyse the diffusion penetration profile in terms of lattice diffusion and short-circuit diffusion terms:

$$C(x,t) = \frac{M}{\sqrt{\pi Dt}} \exp\left(-\frac{x^2}{4Dt}\right) + C_0 \exp(-A\ x^{6/5})\,. \tag{13.9}$$

   Here C_0 is constant, which depends on the density of grain boundaries. The quantity A is related to the grain-boundary diffusivity, the grain-boundary width, and to the lattice diffusivity. The grain-boundary tails can be used for a systematic study of grain-boundary diffusion in bi- or polycrystalline samples. Grain-boundary diffusion is discussed in Chap. 32.
2. *Evaporation losses of tracer*: A tracer with high vapour pressure will simultaneously evaporate from the surface and diffuse into the sample. Then, the thin-film solution (13.4) is no longer valid. The outward flux of the tracer will be proportional to the tracer concentration at the surface:

$$D\left(\frac{\partial C}{\partial x}\right)_{x=0} = -KC(0)\,. \tag{13.10}$$

K is the rate constant for evaporation. The solution for Fick's second equation for this boundary condition is [1]

$$C(x,t) = M\left[\frac{1}{\sqrt{\pi Dt}}\exp\left(-\frac{x^2}{4Dt}\right) - \frac{K}{D}\exp\left(\frac{K^2}{D^2}Dt + \frac{K}{D}x\right)\right.$$
$$\left.\operatorname{erfc}\left(\frac{x}{2\sqrt{Dt}} + \frac{K}{D}\sqrt{Dt}\right)\right] . \tag{13.11}$$

Evaporation losses of the tracer cause negative deviations from Gaussian behaviour in the near-surface region.

3. *Evaporation losses of the matrix*: For a matrix material with a high vapour pressure the surface of the sample may recede due to evaporation. A solution for continuous matrix removal at a rate v and simultaneous in-diffusion of the tracer has been given by [20]

$$C(x',t) = M\left[\frac{1}{\sqrt{\pi Dt}}\exp(-\eta^2) - \frac{v}{2D}\operatorname{erfc}(\eta)\right] , \tag{13.12}$$

where x' is the distance from the surface after diffusion and $\eta = (x' + vt)/2\sqrt{Dt}$.

13.3.2 Residual Activity Method

Gruzin has suggested a radiotracer technique, which is called the residual activity method [21]. Instead of analysing the activity in each removed section, the activity remaining in the sample after removing a section is measured. This method is applicable if the radiation being detected is absorbed exponentially. The residual activity $A(x_n)$ after removing a length x_n from the sample is then given by

$$A(x_n) = k\int_{x_n}^{\infty} C(x)\exp[-\mu(x - x_n)]\mathrm{d}x , \tag{13.13}$$

where k is a constant and μ is the absorption coefficient. According to Seibel [22] the general solution of Eq. (13.13) – independent of the functional form of $C(x)$ – is given by

$$C(x_n) = kA(x_n)\left[\mu - \frac{\mathrm{d}\ln A(x_n)}{\mathrm{d}x_n}\right] . \tag{13.14}$$

If the two bracket terms in Eq. (13.14) are comparable, the absorption coefficient must be measured accurately in the same geometry in which the sample is counted. Thus, the Gruzin method is less desirable than counting the sections, except for two limiting cases:

1. *Strongly absorbed radiation*: Suppose that the radiation is so weak that it is absorbed in one section, i.e. $\mu \gg \mathrm{d}\ln A(x_n)/\mathrm{d}x_n$. Isotopes such as ^{63}Ni,

^{14}C, or ^{3}H emit weak β-radiation. Their radiation is readily absorbed and Eq. (13.14) reduces to

$$C(x_n) = \mu k A(x_n) \tag{13.15}$$

and the residual activity $A(x_n)$ follows the same functional form as $C(x_n)$. In this case, the Gruzin technique has the advantage that it obviates the tedious preparation of sections for counting.

2. *Slightly absorbed radiation*: For $\mu \ll \mathrm{d}\ln A(x_n)/\mathrm{d}x_n$ the radiation is so energetic that absorption is negligible. Then, the activity A_n in section n is obtained by subtracting two subsequent residual activities:

$$A_n = A(x_n) - A(x_{n+1})\,. \tag{13.16}$$

The Gruzin technique is useful, when the specimen can be moved to the counter repeatedly without loosing alignment in the sectioning device. In general, this method is not as reliable as sectioning and straightforward measurement of the section activity.

13.4 Isotopically Controlled Heterostructures

The use of enriched stable isotopes combined with modern epitaxial growth techniques enables the preparation of isotopically controlled heterostructures. Either chemical vapour deposition (CVD) or molecular beam epitaxy (MBE) are used to produce the desired heterostructures. After diffusion annealing, the diffusion profiles can be studied using, for example, conventional SIMS or TOF-SIMS techniques (see the next section).

We illustrate the benefits of this method with an example of Si self-diffusion. In the past, self-diffusion experiments were carried out using the radiotracer ^{31}Si with a half-life of 2.6 hours. However, this short-lived radiotracer limits such studies to a narrow high-temperature range near the melting temperature of Si. Other self-diffusion experiments utilising the stable isotope ^{30}Si (natural abundance in Si is about 3.1 %) in conjunction with neutron activation analysis, SIMS profiling and nuclear reaction analysis (NRA) overcame this diffuculty (see also Chap. 23). However, these methods have the disadvantage that the ^{30}Si background concentration is high.

Figure 13.7 illustrates the technique of isotopically controlled heterostructures for Si self-diffusion studies. The sample consists of a Si-isotope heterostructure, which was grown by chemical vapour deposition on a natural floating-zone Si substrate. A 0.7 µm thick ^{28}Si layer was covered by a layer of natural Si (92.2 % ^{28}Si, 4.7 % ^{29}Si, 3.1 % ^{30}Si). The ^{28}Si profile in the as-grown state (dashed line), after a diffusion anneal (crosses), and the best fit to the data (solid line) are shown. Diffusion studies on isotopically controlled heterostructures have been used by Bracht and Haller and their associates mainly for self- and dopant diffusion studies in elemental [24, 25] and compound semiconductors [26–28].

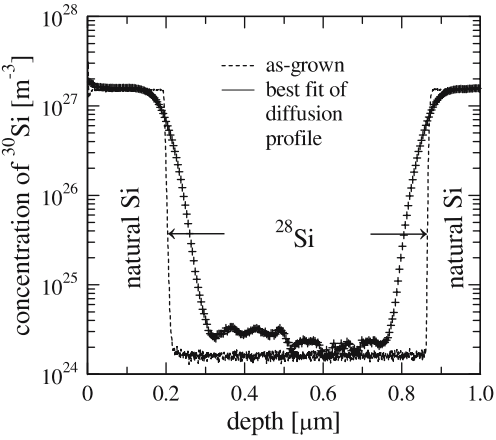

Fig. 13.7. SIMS depth profiles of ^{30}Si measured before and after annealing at 925 °C for 10 days of a ^{28}Si isotope heterostructure. The initial structure consisted of a layer of ^{28}Si embedded in natural Si

13.5 Secondary Ion Mass Spectrometry (SIMS)

Secondary ion mass spectroscopy (SIMS) is an analytical technique whereby layers of atoms are sputtered off from the surface of a solid, mainly as neutral atoms and a small fraction as ions. Only the latter can be analysed in a mass spectrometer. Several aspects of the sputtering process are illustrated in Fig. 13.8. The primary ions (typically energies of a few keV) decelerate during impact with the target by partitioning their kinetic energy through a series of collisions with target atoms. The penetration depth of the primary ions depends on their energy, on the types of projectile and target atoms and their atomic masses, and on the angle of incidence. Each primary ion initiates a 'collision cascade' of displaced target atoms, where momentum vectors can be in any direction. An atom is ejected after the sum of phonon and collisional energies focused on a target atom exceeds some threshold energy. The rest of the energy dissipates into atomic mixing and heating of the target.

The sputtering yield of atomic and molecular species from a surface depends strongly on the target atoms, on the primary ions and their energy. Typical yields vary between 0.1 to 10 atoms per primary ion. The great majority of emitted atoms are neutral. For noble gas primaries the percentage of secondary ions is below 1 %. If one uses reactive primary ions (e.g., oxygen- or alkali-ions) the percentage of secondary ions can be enhanced through the interaction of a chemically reactive species with the sputtered species by exchanging electrons.

In a SIMS instrument, schematically illustrated in Fig. 13.9, a primary ion beam hits the sample. The emitted secondary ions are extracted from the surface by imposing an electrical bias of a few kV between the sample

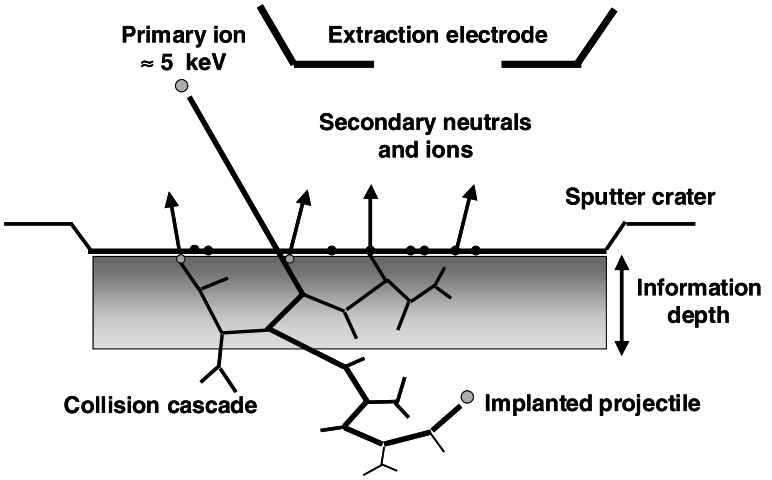

Fig. 13.8. Sputtering process at a surface of a solid

and the extraction electrode. The secondary ions are then transferred to the spectrometer via a series of electrostatic and magnetic lenses. The spectrometer filters out all but those ions with the chosen mass/charge ratios, which are then delivered to the detector for counting. The classical types of mass spectrometers are equipped either with quadrupole filters, or electric and magnetic sector fields.

Time-of-flight (TOF) spectrometers are used in TOF-SIMS instruments. The TOF-SIMS technique developed mainly by Benninghoven [35] combines high lateral resolution ($< 60\,\mathrm{nm}$) with high depth resolution ($< 1\,\mathrm{nm}$). It is nowadays acknowledged as one of the major techniques for the surface characterisation of solids. In different operational modes - surface spectrometry, surface imaging, depth profiling - this technique offers several features: the mass resolution is high; in principle all elements and isotopes can be detected and also chemical information can be obtained; detection limits in the range of ppm of a monolayer can be achieved. For details of the construction of SIMS devices we refer to [33, 34, 36, 37].

When SIMS is applied for diffusion profile measurements, the mass spectrum is scanned and the ion current for tracer and host atoms can be recorded simultaneously. In conventional SIMS, the ion beam is swept over the sample and, in effect, digs a crater. An aperture prevents ions from the crater edges from reaching the mass spectrometer. The diffusion profile is constructed from the plots of instantaneous tracer/host atom ratio *versus* sputtering time. The distance is deduced from a measurement of the total crater depth, assuming that the material is removed uniformly as a function of time. Large changes of the chemical composition along the diffusion direction can invalidate this assumption.

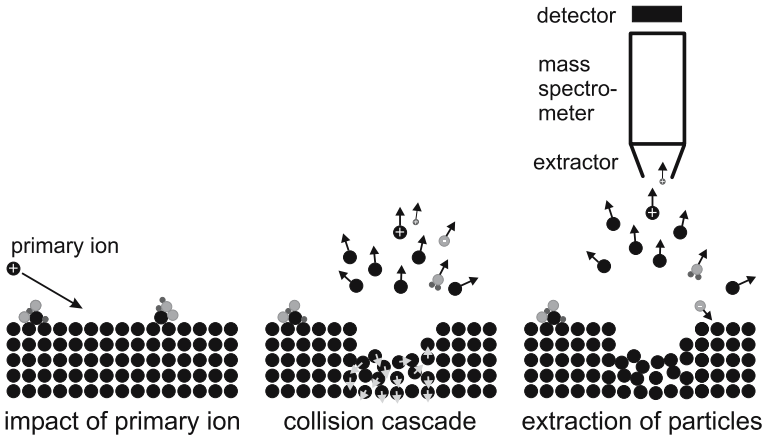

Fig. 13.9. SIMS technique (schematic illustration)

One must keep in mind that the relationship between measured secondary-ion signals and the composition of the target is complex. It involves all aspects of the sputtering process. These include the atomic properties of the sputtered ions such as ionisation potentials, electron affinities, the matrix composition of the target, the environmental conditions during the sputtering process such as the residual gas components in the vacuum chamber, and instrumental factors. Diffusion analysis by SIMS also depends on the accuracy of measuring the depth of the eroded crater and the resolution of the detected concentration profile. A discussion of problems related to quantification and standardisation of composition and distance in SIMS experiments can be found in [34, 39].

SIMS, like the IBS technique discussed above, enables the measurement of very small diffusion coefficients, which are not attainable with mechanical sectioning techniques. The very good depth resolution and the high sensitivity of mass spectrometry allows the resolution of penetration profiles of solutes in the 10 nm range and at ppm level. Several perturbing effects, inherent to the method and limiting its sensitivity are: degradation of depth resolution by surface roughening, atomic mixing, and near surface distortion of profiles by transient sputtering effects.

SIMS has mainly been applied for diffusion of foreign atoms although the high mass resolution especially of TOF-SIMS also permits separation of stable isotopes of the same element. SIMS has found particularly widespread use in studies of implantation- and diffusion profiles in semiconductors. However, SIMS is applicable to all kinds of solids. As an example, Fig. 13.10 shows diffusion profiles for both stable isotopes ^{69}Ga and ^{71}Ga of natural Ga in a ternary Al-Pd-Mn alloy (with a quasicrystalline structure) according to [38]. For metals, the relatively high impurity content of so-called 'pure metals' as compared to semiconductors can limit the dynamic range of SIMS profiles.

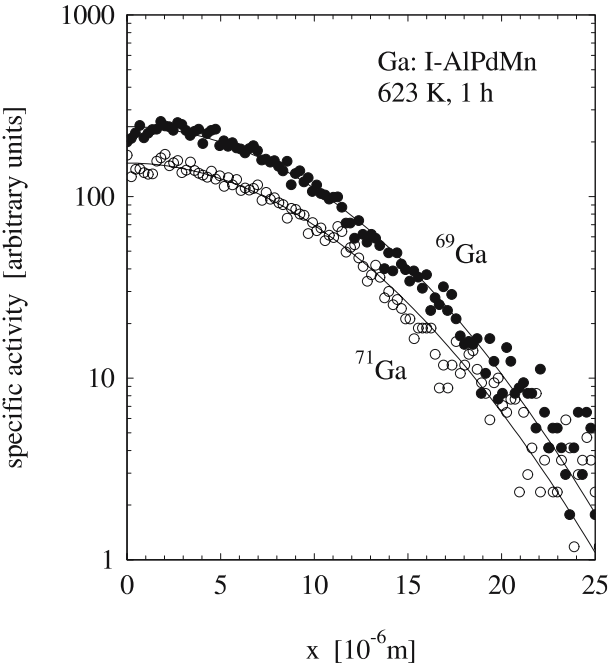

Fig. 13.10. Diffusion profiles for both stable isotopes ^{69}Ga and ^{71}Ga of natural Ga in AlPdMn (icosahedral quasicrystalline alloy) according to [38]. The *solid lines* represent fits of the thin-film solution

SIMS has in few cases also been applied to self-diffusion. This requires that highly enriched stable isotopes are available as tracers. Contrary to self-diffusion studies by radiotracer experiments, in the case of stable tracers diffused into a matrix with a natural abundance of stable isotopes the latter limits the concentration range of the diffusion profile. A fine example of this technique can be found in a study of Ni self-diffusion in the intermetallic compound Ni_3Al, in which the highly enriched stable ^{64}Ni isotope was used [40]. The limitation due to the natural abundance of a stable isotope in the host has been avoided in some SIMS studies of self-diffusion on amorphous Ni-containing alloys by using the radioisotope ^{63}Ni as tracer [42, 43].

An elegant possibility to overcome the limits posed by the natural abundance of stable isotopes are isotopically controlled heterostructures. This method is discussed in the previous section and illustrated in Fig. 13.7.

13.6 Electron Microprobe Analysis (EMPA)

The basic concepts of electron microprobe analysis (EMPA) can be found already in the PhD thesis of Castaing [44]. The major components of an

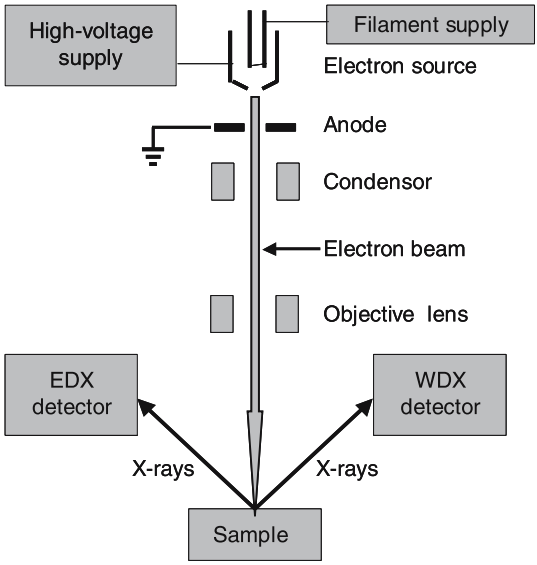

Fig. 13.11. Schematic view of an electron microprobe analyser (EMPA)

EMPA equipment are illustrated in Fig. 13.11. An electron-optical column containing an electron gun, magnetic lenses, a specimen chamber, and various detectors is maintained under high vacuum. The electron-optical column produces a finely focused electron beam, with energies ranging between 10 and 50 keV. Scanning coils and/or a mechanical scanning device for the specimen permit microanalysis at various sample positions. When the beam hits the specimen it stimulates X-rays of the elements present in the sample. The X-rays are detected and characterised either by means of an energy dispersive X-ray spectrometer (EDX) or a crystal diffraction spectrometer. The latter is also referred to as a wave-length dispersive spectrometer (WDX).

The ability to perform a chemical analysis is the result of a simple and unique relationship between the wavelength of the characteristic X-rays, λ, emitted from an element and its atomic number Z. It was first observed by Moseley [45] in 1913. He showed that for K radiation

$$Z \propto \frac{1}{\sqrt{\lambda}}. \tag{13.17}$$

The origin of the characteristic X-ray emission is illustrated schematically in Fig. 13.12. An incident electron with sufficient energy ejects a core electron from its parent atom leaving behind an orbital vacancy. The atom is then in an excited state. Orbital vacancies are quickly filled by electronic relaxations accompanied by the release of a discrete energy corresponding to the difference between two orbital energy levels. This energy can be emitted as an X-ray photon or it can be transferred to another orbital electron, called

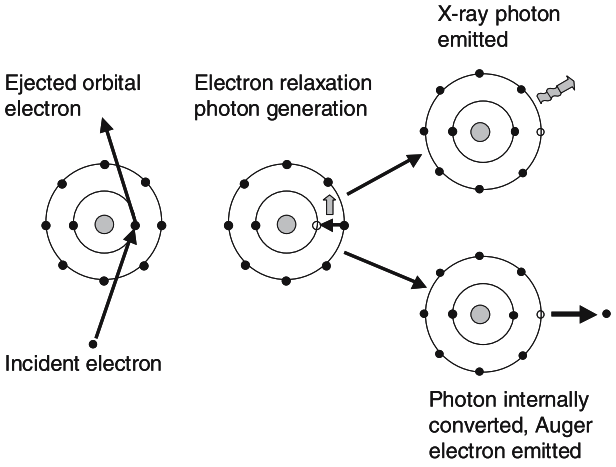

Fig. 13.12. Characteristic X-ray and Auger-electron production

an Auger electron, which is ejected from the atom. The fraction of electronic relaxations which result in X-ray emission rather than Auger emission depends strongly on the atomic number. It is low for small atomic numbers and high for large atomic numbers. The characteristic radiation is superimposed to the continuous radiation also denoted as 'Bremsstrahlung'. The continuum is the major source of the background and the principal factor limiting the X-ray sensitivity. For details about EMPA, the reader may consult, e.g., the reviews of Hunger [46] and Lifshin [47].

A diffusion profile is obtained by examining on a polished cross-section of a diffusion sample the intensity of the characteristic radiation of the element(s) involved in the diffusion process along the diffusion direction. The detection limit in terms of atomic fractions is about 10^{-3} to 10^{-4}, depending on the selected element. It decreases with decreasing atomic number. Light elements such as C or N are difficult to study because their fluorescence yield is low. The diameter of the electron beam is typically 1 μm or larger depending on the instrument's operating conditions. Accordingly, the volume of X-ray generation is of the order of several μm^3. This limits the spatial resolution to above 1 to 2 μm. Thus, only relatively large diffusion coefficients $D > 10^{-15}\,m^2\,s^{-1}$ can be measured (Fig. 13.1). Because of its detection limit, EMPA is mainly appropriate for interdiffusion- and multiphase-diffusion studies. An example of a single-phase interdiffusion profile for an $Al_{50}Fe_{50}$–$Al_{30}Fe_{70}$ couple is shown in Fig. 13.13 [23].

The Boltzmann-Matano method [29, 30] is usually employed to evaluate interdiffusion coefficients $\tilde{D}$ from an experimental profile. Related procedures for non-constant volume have been developed by Sauer and Freise and den Broeder [31, 32]. These methods for deducing the interdiffusion coefficient, $\tilde{D}(c)$, from experimental concentration-depth profiles are described in Chap. 10.

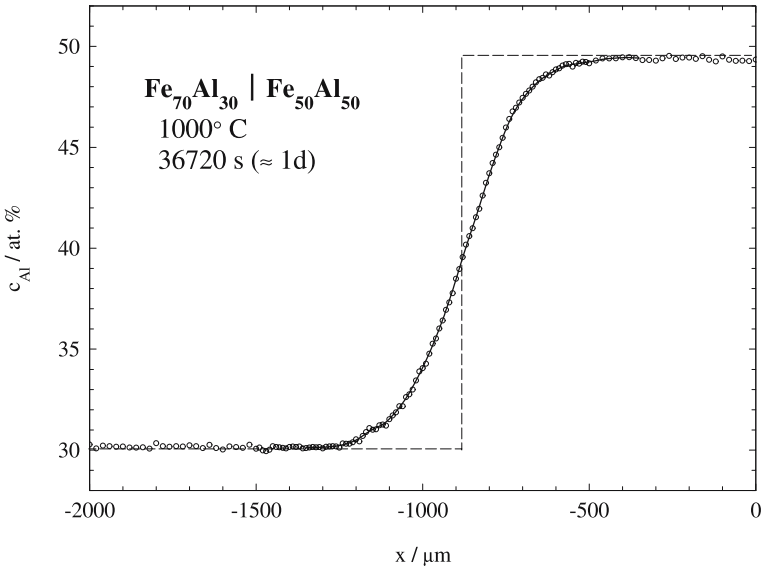

Fig. 13.13. Interdiffusion profile of a $Fe_{70}Al_{30}$–$Fe_{50}Al_{50}$ couple measured by EMPA according to SALAMON ET AL. [23]. *Dashed line*: composition distribution before the diffusion anneal

13.7 Auger-Electron Spectroscopy (AES)

Auger-electron spectroscopy (AES) is named after PIERRE AUGER, who discovered and explained the Auger effect in experiments with cloud chambers in the mid 1920s (see [48]). An Auger electron is generated by transitions within the electron orbitals of an atom following an excitation an electron from one of the inner levels (see Fig. 13.12). Auger-electron spectroscopy (AES) was introduced in the 1960s. In AES instruments the excitation is performed by a primary electron beam.

The kinetic energy of the Auger electron is independent of the primary beam but is characteristic of the atom and electronic shells involved in its production. The probability that an Auger electron escapes from the surface region decreases with decreasing kinetic energy. The range of analytical depth in AES is typically between 1 and 5 nm. AES is one of the major techniques for surface analysis.

When a primary electron beam strikes a surface, Auger electrons are only a fraction of the total electron yield. Most of the electrons emitted from the surface are either secondary electrons or backward scattered electrons. These and the inelastically scattered Auger electrons constitute the background in an Auger spectrum. Auger-electron emission and X-ray fluorescence after creation of a core hole are competing processes and the emission probability depends on the atomic number. The probability for Auger-electron emission

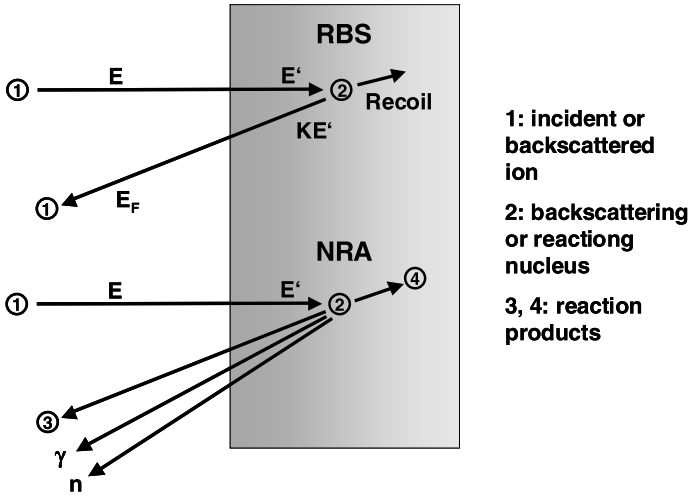

Fig. 13.14. Schematic representation of Rutherford backscattering (RBS) and of nuclear reaction analysis (NRA)

decreases with increasing atomic number whereas the probability for X-ray fluorescence increases with atomic number. AES is thus particularly well suited for light elements.

The combined operation of an AES spectrometer for chemical surface analysis and an ion sputtering device can be used for depth profiling. Information with regard to the quantification and to factors affecting their resolution can be found, e.g., in [49, 50]. AES is applicable to diffusion of foreign atoms, since AES only discriminates between different elements. It has, for example, been used to measure Au and Ag diffusion in amorphous Cu-Zr [41] and Cu and Al diffusion in amorphous $Zr_{61}Ni_{39}$-alloys [51].

13.8 Ion-beam Analysis: RBS and NRA

High-energy ion-beam analysis has several desirable features for depth profiling of diffusion samples. The technique is largely non-destructive, it offers good depth resolution, and measurements of both concentration and depth can be achieved. The depth resolution is in the range from about 0.01 to 1 μm. This is inferior to the depth resolution achieved in IBS or SIMS devices but substantially better than the resolution of mechanical sectioning techniques.

Atomic species are identified in ion-beam analysis by detecting the products of nuclear interactions, which are created by the incident MeV ions. There are several different techniques. The two more important ones are *Rutherford backscattering* (RBS) and *nuclear reaction analysis* (NRA). These two are depicted schematically in Fig. 13.14.

Rutherford Backscattering (RBS): The first scattering experiment was performed by RUTHERFORD in 1911 [53] and his students GEIGER AND MARSDEN [54] for verifications of the atomic model. A radioactive source of α-particles was used to provide energetic probing ions and the particles scattered from a gold foil were observed with a zinc blende scintillation screen. Nowadays, elastic backscattering analysis also denoted as Rutherford backscattering (RBS) is probably the most frequently used ion-beam analytical technique among the surface analysis tools.

In RBS experiments a high-energy beam of monoenergetic ions (usually α-particles) with energies of some MeV is used for depth profiling. The sample is bombarded along the diffusion direction with ions and one studies the number of elastically backscattered ions as a function of their energy. The particles of the analysing beam are scattered by the nuclei in the sample and the energy spectrum of scattered particles is used to determine the concentration profile of scattering nuclei. The signals from different nuclei can be separated in the energy spectrum, because of the different kinematic factors K of the scattering process. K is related to the masses of analysing particles and scattering nuclei. It is a monotonically decreasing function of the mass of the target nuclei. The backscattered particles re-emerge unchanged except for a reduction in energy. The depth information comes from the continuous energy loss of the ions in the sample. The yield of the backscattered ions is proportional to the concentration of the scattering nuclei.

RBS is illustrated schematically in Fig. 13.15 for a layer of heavy atoms (mass M) deposited on a substrate of light atoms (Mass m). Yield and energy of the backscattered ions are monitored by an energy-sensitive particle detector and a multichannel analyser. The high energy end of the spectrum (M-signal) corresponds to ions backscattered from heavy atoms at the sample surface. The low energy end of the M-signal corresponds to ions backscattered from the heavy atoms near the interface. The signals from the heavy and light nuclei are separated in the spectrum due to the different kinematic factors for heavy and light nuclei.

Although widely applicable, RBS has two inherent limitations for diffusion studies: First, the element of interest must differ in mass sufficiently – at least several atomic masses – from other constituents of the sample. Second, adequate sensitivity is achieved only when the solutes are heavier than the majority constituents of the matrix. Then, the backscattering yield from the diffuser appears at higher energies than the yield from the majority nuclei. Therefore, RBS is particular suitable for detecting heavy elements in a matrix of substantially lower atomic weight. Because of the limited penetration range of ions (several micrometers) and the associated energy straggling in a solid, only relatively small diffusion coefficients are accessible.

Nuclear Reaction Analysis (NRA): In a NRA profiling experiment monoenergetic high-energy particles (protons, α-particles, ...) are used as in RBS. NRA is applicable if the analysing particles undergo a suitable nu-

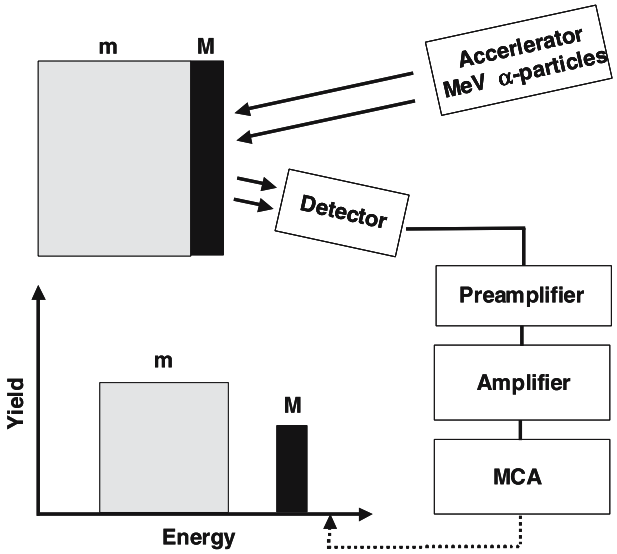

Fig. 13.15. Rutherford backscattering spectrometry: high-energy ion beam, electronics for particle detection and a schematic example of a RBS spectrum. The technique is illustrated for a thin layer of atoms with mass M deposited on a substrate of lower mass m

clear reaction with narrow resonance with the atoms of interest. The yield of out-going reaction products is measured as a function of the energy of the incident beam. From the yield *versus* energy curve the concentration profile can be deduced.

As shown schematically in Fig. 13.14, the analysis-beam particles undergo an inelastic, exothermic nuclear reaction with the target nuclei thus producing two or more new particles. Depending on the conditions it may be preferable to detect either charged reaction products, neutrons or γ-rays from the reaction. This method distinguishes specific isotopes and is therefore free from the mass-related restrictions of RBS. Suitable resonant nuclear reactions occur for at least one readily available isotope of all elements from hydrogen to fluorine and for beam energies below 2 MeV. NRA can mainly be used to investigate the diffusion of light solutes in a heavier matrix.

Concluding Remarks: Depth profiling is possible in RBS and NRA because the charged particles continuously loose energy as they traverse the specimen. Usually, this loss is almost entirely due to electronic excitations, although there is some additional contribution from small-angle nuclear scattering. The consequences may be appreciated by considering the RBS experiment illustrated in Fig. 13.15. In RBS the energy of the analysis-beam particle decreases during both inward and outward passages. When the particle is detected, the accumulated energy loss is superimposed on the recoil

loss via the kinematic factor. Hence the measured energy decreases monotonically with the depth of the scattering nucleus. In NRA the situations are analogous but more varied. For example, the relevant energy loss may occur only during the inward or outward passage. Nevertheless, depth resolution is always a consequence of the charged-particle energy loss in the sample. For example, the diffusion of ion-implanted boron in amorphous $Ni_{59.5}Nb_{40.5}$ was measured by irradiating the amorphous alloy with high energy protons and detecting α-particles emitted from the nuclear reaction $^{11}B + p \rightarrow {}^{8}B + \alpha$, and determining the concentration profile of ^{11}B from the number and energy of emitted α-particles as a function of the incident proton energy [52].

In NRA and in RBS the penetration range of ions is not more than several micrometer. This limits the diffusion depth. Diffusion coefficients between about 10^{-17} and $10^{-23}\,m^2\,s^{-1}$ are accessible (see also Fig. 13.1). Both RBS and NRA methods need a depth calibration, which is based on not always very accurate data of the stopping power in the matrix for the relevant particles. Also the depth resolution is usually inferior to that achievable in careful IBS radiotracer and SIMS profiling studies. For a comprehensive discussion of ion-beam techniques the reader may consult reviews by Myers [55], Lanford et al. [56], and Chu et al. [57].

References

1. J. Crank, *The Mathematics of Diffusion*, Oxford University Press, 2nd ed., 1975
2. J. Philibert, *Atom Movements – Diffusion and Mass Transport in Solids*, Les Editions de Physique, Les Ulis, 1991
3. Th. Heumann, *Diffusion in Metallen*, Springer-Verlag, Berlin, 1992
4. S.J. Rothman, *The Measurement of Tracer Diffusion Coefficients in Solids*, in: *Diffusion in Crystalline Solids*, G.E. Murch, A.S. Nowick (Eds.), Academic Press, 1984, p. 1
5. H. Mehrer (Vol. Ed.), Sect. 1.6 in: *Diffusion in Solid Metals and Alloys*, Landolt-Börnstein, Numerical Data and Functional Relationships in Science and Technology, New Series, Group III: Crystal and Solid State Physics, Vol. 26, Springer-Verlag, 1990
6. Proc. Int. Conf. on *Diffusion in Materials – DIMAT-92*, Kyoto, Japan, 1992, M. Koiwa, H. Nakajima, K.-I. Hirano (Eds.); also: Defect and Diffusion Forum **95–98** (1993)
7. Proc. Int. Conf. on *Diffusion in Materials – DIMAT-96*, Nordkirchen, Germany, 1996, H. Mehrer, Chr. Herzig, N.A. Stolwijk, H. Bracht (Eds.); also: Defect and Diffusion Forum **143–147** (1997)
8. Proc. Int. Conf. on *Diffusion in Materials – DIMAT-2000*, Paris, France, 2000, Y. Limoge, J.L. Bocquet (Eds.); also: Defect and Diffusion Forum **194–199** (2001)
9. Proc. Int. Conf. on *Diffusion in Materials – DIMAT-2004*, Cracow, Poland, 2004, M. Danielewski, R. Filipek, R. Kozubski, W. Kucza, P. Zieba, Z. Zurek (Eds.); also: Defect and Diffusion Forum **237–240** (2005)
10. H. Mehrer, Materials Transactions, JIM, **37**, 1259 (1996)

11. H. Mehrer, F. Wenwer, *Diffusion in Metals*, in: *Diffusion in Condensed Matter*, J. Kärger, R. Haberlandt, P. Heitjans (Eds.), Vieweg Verlag, 1998
12. H. Mehrer, *Diffusion: Introduction and Case Studies in Metals and Binary Alloys*, in: *Diffusion in Condensed Matter – Methods, Materials, Models*, P. Heitjans, J. Kärger (Eds.), Springer-Verlag, 2005
13. D. Tannhauser, J. Appl. Phys. **27**, 662 (1956)
14. H. Mehrer, Phys. Stat. Sol. (a) **104**, 247 (1987)
15. A. Gude, H. Mehrer, Philos. Mag. A **76**, 1 (1996)
16. F. Faupel, P.W. Hüppe, K. Rätzke, R. Willecke. T. Hehenkamp, J. Vac. Sci. Technol. a **10**, 92 (1992)
17. F. Wenwer, A. Gude, G. Rummel, M. Eggersmann, Th. Zumkley, N.A. Stolwijk, H. Mehrer, Meas. Sci. Technol. **7**, 632 (1996)
18. M. Eggersmann, B. Sepiol, G. Vogl, H. Mehrer, Defect and Diffusion Forum **143–147**, 339 (1997)
19. I. Kaur, Y. Mishin, W. Gust, *Fundamentals of Grain and Interphase Boundary Diffusion*, John Wiley & Sons Ltd., 1995
20. R.N. Ghoshtagore, Phys. Stat. Sol. **19**, 123 (1967)
21. P.L. Gruzin, Dokl. Akad. Nauk. SSSR **86**, 289 (1952)
22. G. Seibel, Int. J. Appl. Radiat. Isot. **15**, 679 (1964)
23. M. Salamon, S. Dorfman, D. Fuks, G. Inden, H. Mehrer, Defect and Diffusion Forum **194–199**, 553 (2001)
24. H.D. Fuchs, W. Walukiewicz, E.E. Haller, W. Dondl, R. Schorer, G. Abstreiter, A.I. Rudnev, A.V. Tikomirov, V.I. Ozhogin, Phys. Rev. **B 51**, 16817 (1995)
25. H. Bracht, E.E. Haller, R. Clark-Phelps, Phys. Rev. Lett. **81** 393 (1998)
26. L. Wang, L. Hsu, E.E. Haller, J.W. Erickson, A. Fisher, K. Eberl, M. Cardona, Phys. Rev. Lett. **76**, 2342 (1996)
27. L. Wang, J.A. Wolk, L. Hsu, E.E. Haller, J. W. Erickson, M. Cardona, T. Ruf, J.P. Silveira, F. Briones, Appl. Phys. Lett. **70**, 1831 (1997)
28. H. Bracht, E.E. Haller, K. Eberl, M. Cardona, R. Clark-Phelps, Mat. Res. Soc. Symp. **527**, 335 (1998)
29. L. Boltzmann, Wiedemanns Ann. Physik **53**, 959 (1894)
30. C. Matano, Jap. J. Phys. **8**, 109–113 (1933)
31. F. Sauer, V. Freise, Z. Elektrochem. **66**, 353 (1962)
32. F.J.A. den Broeder, Scr. Metall. **3**, 321 (1969)
33. C.-E. Richter, *Sekundärionen-Massenspektroskopie und Ionenstrahl-Mikroanalyse*, in: *Ausgewählte Untersuchungsverfahren der Metallkunde*, H.-J. Hunger et al. (Eds.), VEB Verlag, 1983, p. 197
34. W.T. Petuskey, *Diffusion Analysis using Secondary Ion Mass Spectroscopy*, in: *Nontraditional Methods in Diffusion*, G.E. Murch, H.K. Birnbaum, J.R. Cost (Eds.), The Metallurgical Society of AIME, Warrendale, 1984, p. 179
35. A. Benninghoven, *The History of Static SIMS: a Personal Perspective*, in: *TOF-SIMS – Surface Analysis by Mass Spectrometry*, J.C. Vickerman, D. Briggs (Eds.), IM Publications and Surface Spectra Limited, 2001
36. A. Benninghoven, F.G. Rüdenauer, H.W. Werner, *Secondary Ion Mass Spectrometry – Basic Concepts, Instrumental Aspects, Applications and Trends*, John Wiley and Sons, Inc., 1987
37. J.C. Vickerman, D. Briggs (Eds.), *TOF-SIMS – Surface Analysis by Mass Spectrometry*, IM Publications and Surface Spectra Limited, 2001

38. H. Mehrer, R. Galler, W. Frank, R. Blüher, T. Strohm, *Diffusion in Quasicrystals*, in: *Quasicrystals: Structure and Physical Properties*, H.-R. Trebin (Ed.), J. Wiley VCH, 2003
39. M.-P. Macht, V. Naundorf, J. Appl. Phys. **53**, 7551 (1982)
40. S. Frank, U. Södervall, Chr. Herzig, Phys. Stat. Sol. (b) **191**, 45 (1995)
41. E.C. Stelter, D. Lazarus, Phys. Rev. B **36**, 9545 (1987)
42. A.K. Tyagi, M.-P. Macht, V. Naundorf, Scripta Metall. et Mater. **24**, 2369 (1999)
43. A.K. Tyagi, M.-P. Macht, V. Naundorf, Acta Metall. et Mater. **39**, 609 (1991)
44. R. Castaing, Ph.D. thesis, Univ. of Paris, 1951
45. H.G.J. Moseley, Philos. Mag. **26**, 1024 (1913)
46. H.-J. Hunger, *Elektronenstrahl-Mikroanalyse und Rasterelektronen-Mikroskopie*, in: *Ausgewählte Untersuchungsverfahren der Metallkunde*, H.-J. Hunger et al. (Eds.), VEB Deutscher Verlag für Grundstoffindustrie, Leipzig, 1983, p.175
47. E. Lifshin, *Electron Microprobe Analysis*, in: *Materials Science and Technology*, R.W. Cahn, P. Haasen, E.J. Kramer (Eds.), Vol. 2B: Characterisation of Materials, VCH, 1994, p. 351
48. P. Auger, Surf. Sci **1**, 48 (1975)
49. S. Hofmann, Surf. Interface Anal. **9**, 3 (1986)
50. A. Zalar, S. Hofmann, Surf. Interface Anal. **12**, 83 (1988)
51. S.K. Sharma, P. Mukhopadhyay, Acta Metall. **38**, 129 (1990)
52. M.M. Kijek, D.W. Palmer, B. Cantor, Acta Metall. **34**, 1455 (1986)
53. E. Rutherford, Philos. Mag. **21**, 669 (1911)
54. H. Geiger, E. Marsden, Philos. Mag. **25**, 206 (1913)
55. S.M. Myers, *Ion-beam Analysis and Ion Implantation in the Study of Diffusion*, in: *Nontraditional Methods in Diffusion*, G.E. Murch, H.K. Birnbaum, J.R. Cost (Eds.), The Metallurgical Society of AIME, Warrendale, 1984, p. 137
56. W.A. Lanford, R. Benenson, C. Burman, L. Wielunski, *Nuclear Reaction Analysis for Diffusion Studies*, in: *Nontraditional Methods in Diffusion*, G.E. Murch, H.K. Birnbaum, J.R. Cost (Eds.), The Metallurgical Society of AIME, Warrendale, 1984, p. 155
57. W.K. Chu, J. Liu, Z. Zhang, K.B. Ma, *High Energy Ion Beam Analysis Techniques*, in: *Materials Science and Technology*, R.W. Cahn, P. Haasen, E.J. Cramer (Eds.), Vol. 2B: Characterisation of Materials, VCH Weinheim, 1994, p. 423